Available online at www.sciencedirect.com

ScienceDirect

Green Energy & Environment 5 (2020) 22–36

www.keaipublishing.com/gee

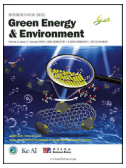

Short Review

Internal failure of anode materials for lithium batteries — A critical review

Xiangqi Meng [a,b,c], Yaolin Xu [c], Hongbin Cao [a,b], Xiao Lin [b], Pengge Ning [b], Yi Zhang [a,b], Yaiza Gonzalez Garcia [d], Zhi Sun [b,*]

[a] School of Chemical Engineering and Technology, Tianjin University, Tianjin, 300350, China
[b] Beijing Engineering Research Centre of Process Pollution Control, Key Laboratory of Green Process and Engineering, Institute of Process Engineering, Chinese Academy of Sciences, Beijing, 100190, China
[c] Soft Matter and Functional Materials, Helmholtz-Zentrum Berlin für Materialien und Energie GmbH, Hahn-Meitner Platz 1, 14109, Berlin, Germany
[d] Department of Materials Science and Engineering, TU Delft, Delft, 2628CD, the Netherlands

Received 29 January 2019; revised 13 September 2019; accepted 20 October 2019
Available online 27 November 2019

Abstract

Prevention of mechanical and finally electrochemical failures of lithium batteries is a critical aspect to be considered during their design and performance, especially for those with high specific capacities. Internal failure is observed as one of the most serious factors, including loss of electrode materials, structure deformation and dendrite growth. It usually incubates from atomic/molecular level and progressively aggravates along with lithiation. Understanding the internal failure is of great importance for developing solutions of failure prevention and advanced anode materials. In this research, different internal failure processes of anode materials for lithium batteries are discussed. The progress on observation technologies of the anode failure is further summarized in order to understand their mechanisms of internal failure. On top of them, this review aims to summarize innovative methods to investigate the anode failure mechanisms and to gain new insights to develop advanced and stable anodes for lithium batteries.

Keywords: Lithium battery; Anode materials; Internal failure

1. Introduction

In recent years, great progress has been made on the development of lithium batteries since they are considered as the best candidates for powering cell phones, laptop computers and electric vehicles [1–9]. Although tremendous improvements have been made in the development of lithium batteries in the capacity and cycle life, durability is a main obstacle that limits the widespread application of lithium-ion batteries [10–16]. Electrode failure is a fundamental cause of the battery performance degradation, where understanding the failure mechanisms of electrodes, both electrochemical and mechanical, is of great importance [17–25]. Compared with cathode materials, the anode material is more vulnerable to cause failure in the life of a battery induced by the formation of solid electrolyte interphase (SEI) layer, dendrite on anode surface and the volume change of anode, which would cause a short circuit inside battery, which leads to a battery failure. The growth of SEI layer on the anode surface increases the charge transfer resistance and the impedance of the anode [26,27]. Meanwhile, the process of lithiation/delithiation aggravates the anode structural changes, which results in the anode fracture and subsequent failure. Anode failure will be investigated in detail by using advanced technology, and then designated anode material could be synthesized, which is a better solution to extend the life of lithium battery.

The graphite anode changes at the interphase between the electrode and electrolyte interphase. The electrolyte

* Corresponding author.
E-mail address: sunzhi@ipe.ac.cn (Z. Sun).

https://doi.org/10.1016/j.gee.2019.10.003

decomposition products form solid electrolyte interphase (SEI) layer which covers on the surface of anode [28]. Lithium ions can permeate SEI layer, which is impermeable for other charged or neutral elements [18]. The graphite anode interacts with the solvent through the SEI layer. The thickness of the surface layer increases during the process of decomposition reaction. The cracks generated on the surface would not develop inside the graphite anode. In this process, the graphite anode materials become instable and fracture gradually due to expansion and contraction. Fig. 1a illustrates working principle of the lithium-ion battery and the process of anode material fracture [29].

Graphite has been widely used as the anode material in lithium-ion batteries because it can remain structural stability relatively during the intercalation and deintercalation process of lithium ion, while the energy density of graphite (372 mA h g^{-1}) cannot meet the need of widespread applications of lithium-ion batteries. Novel anode materials like silicon [31–40], boron [41–46], tin [47–52], and lithium metal [53–59] are considered to be promising materials because of their high specific capacities. However, these anode materials undergo similar or much larger potential of performance failure, which is rather important to be tackled in order to ensure a durable lithium-ion battery set-up. Concerning this feature, it is imperative to find out the failure mechanisms of the anode materials, which concerns the cycle life of lithium-ion battery.

For instance, silicon has been proposed as promising anodes due to its improved energy density and high-capacity. However, the volume change of silicon anode materials can be 300% upon full lithiation [60–65]. Fig. 1b demonstrates that the lithiation expansion leads to crack initiation from the particle surface [19,30]. These excessive volumetric changes induce irreversible anode cracking, fracture and pulverization. Consequently, the mechanical failure of anode results in capacity decay, significantly shortening the cycle life [13,17,60,66].

This review is organized as follows: First, we discuss different failure processes of anode materials for lithium-ion batteries and summarize the progresses on observation methods of the anode failure in order to understand their mechanisms of cracks, fracture, and failure. Subsequently, advances in suppressing the anode failure are reviewed and analyzed. By means of aggregating and discussing these investigations, this review tries to provide innovative methods to detect the anode failure mechanisms and new insights for the future study of anode materials to optimize the performance of lithium-ion batteries.

Table 1
Summary of different failure types for anode materials in lithium-ion batteries.

Anode failure type		Failure feature
Internal factor	Loss of electrode materials	Irreversible SEI layer
	Structure deformation	Volume change, fracture and delamination
	Dendrite growth	Dendrite growth for Li metal anodes
External factor	Temperature	Side reaction and lithium precipitation
	Ageing	Current collector corrosion and other physical and chemical damages

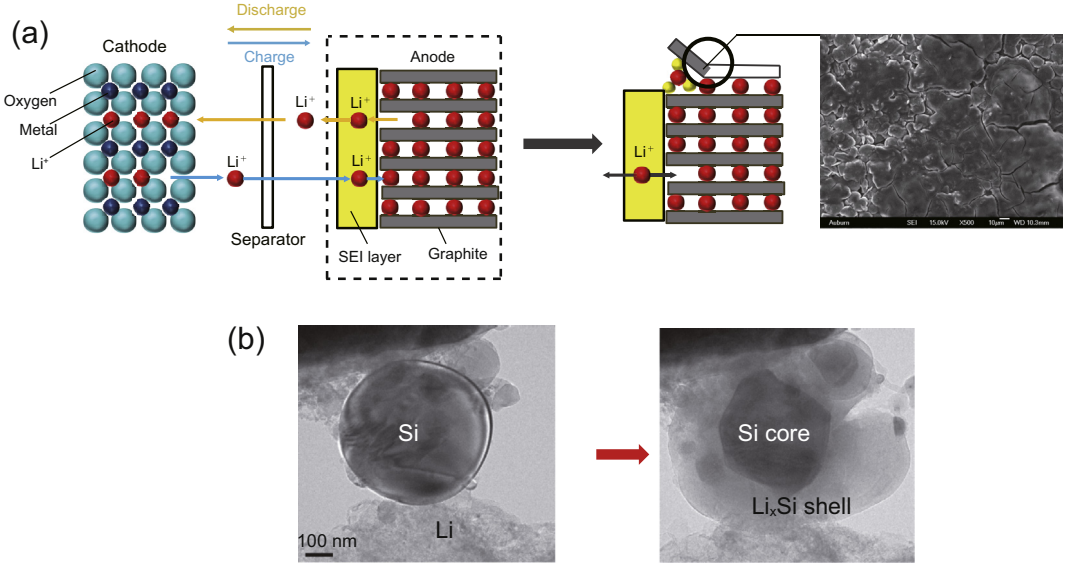

Fig. 1. (a) Schematic illustration of lithium-ion battery and graphite anode fracture, (b) Silicon anode facture by using *in situ* TEM (reprinted with permission from Ref [30] @ copyright 2013 Elsevier).

2. Anode internal failure

2.1. Internal failure types of anode material

Anode material failure would be caused by internal and external factors, which are listed in Table 1. Internal failures are directly correlated to the features of anode materials to be preventable through material design, which are caused by loss of electrode materials, structure deformation and dendrite growth. This review will mainly focus on internal failure of anode material, including irreversible SEI layer, volume change, fracture, delamination, and lithium metal dendrite growth.

2.1.1. Loss of electrode materials

The formation of irreversible SEI layer is considered as a crucial factor of the anode failure [29]. During the first cycle, SEI layer formed at the electrolyte/anode interface. The reaction of the anode with the electrolyte results in the formation of compounds on the anode surface, such as $ROCO_2Li$ and CO_2OLi. Meanwhile, the formation of SEI layer causes the loss of the lithium ion, which decreases the reversible capacity and the Coulombic efficiency of the anode material. The SEI layer could not directly cause mutational failure but an abrasion failure could result in increasing the resistance and reducing the capacity of the battery.

2.1.2. Structure deformation

After multiple cycles, structure deformation of anode would take place, including volume change, fracture and delamination (Fig. 2). When lithium ions penetrate into the anode, Li compound or alloys can be generated, such as LiC_6, and $Li_{22}Si_5$. The reaction can be expressed in the form of equation:

$$X + nLi^+ + ne^- \leftrightarrow Li\,compound/alloy \quad (1)$$

X represents anode element, such as C, and Si, $n \geq 0$. During the insertion and deinsertion of the lithium ions, expansion and contraction occur in the anode material, which leads to the volumetric changes. Subsequently, cracks are gradually formed, resulting in the anode fracture (Fig. 2).

As a result, anode failure takes place inevitably and reduces the cycle life of the lithium-ion battery. It is indicated that the volume of the graphite anode increases by 10% after full lithiation [69]. Tin (1000 mA h g^{-1}) [70], aluminum (2200 mA h g^{-1}) and silicon (4200 mA h g^{-1}) have high specific capacity compared with graphite (372 mA h g^{-1}). However, the volumetric changes of these novel anode materials range from 30% to 100% [71]. Especially for the silicon anode, the volume expansion can be as high as 400% [70] after the full lithiation. This tremendous change in volume is the main factor that restricts the practical application of these promising anode materials.

2.1.3. Dendrite growth

Additionally, anode failure of lithium-ion battery could also be caused by the formation of lithium dendrite. During the processes of charge and discharge, lithium dendrites gradually accumulate on the anode due to the uneven deposition. The persistent growth of the lithium dendrite is likely to cause the separator penetration [72]. When the lithium dendrites finally connect the cathode and anode, the battery is short-circuited, which leads to fire. The formation and growth of lithium dendrites has been regarded as one of the main reasons for the anode failure. This not only reduces the energy storage and conversion efficiency, but also means a matter of safety, which is a serious obstacle for the practical application of promising anode material.

Based on these investigations, lithium dendrite and SEI formation are two important internal failure mechanisms of anode material in lithium batteries. In accordance to the nature of different anode failures, it is important to design appropriate observation systems to investigate anode failure mechanisms for different types of anode failure. For instance, the generation of lithium intercalation compounds may lead to the volumetric change of anode materials, and this process can be detected by some *in situ* techniques. Consequently, it is essential to summarize the development of different techniques for different anode materials to further reveal the anode failure mechanisms.

2.1.4. Comparison between the failure types

SEI formation originates from the irreversible chemical decomposition of electrolytes and their reactions with the anode materials, leading to the continuous loss of active materials along with cycling. However, it is also noted that a stable SEI on the electrode surface would protect the electrode against aggressive electrolytes and mechanical fracturing.

Structure change gradually results in the electrode fragmentation, increasing internal resistance and loss of electrical contact. The mechanical fracturing also produces a fresh surface exposed to the electrolyte and aggravates the problems related to SEI formation.

Dendrite growth is a fatal factor to lithium batteries as it causes short circuit, tremendously challenging its safe operations. Meanwhile, the dendrite formation is accompanied with both the chemical and mechanical issues, e.g. the SEI formation and structure deformation.

In brief, among these three types of failures, the dendritic lithium growth is the most hazardous and challenging for the stable cycling of lithium batteries.

2.2. Internal failure observation technologie of anode materials

2.2.1. Graphite anode

Graphite anode failure is mainly caused by stress and strain generated in the anode, which induced by the generation of intercalation compounds and binder swelling during repeated cycling [73–75]. These factors may lead to volume change and performance degradation [74,76,77]. To investigate the mechanical failure of the anode material, it is crucial to

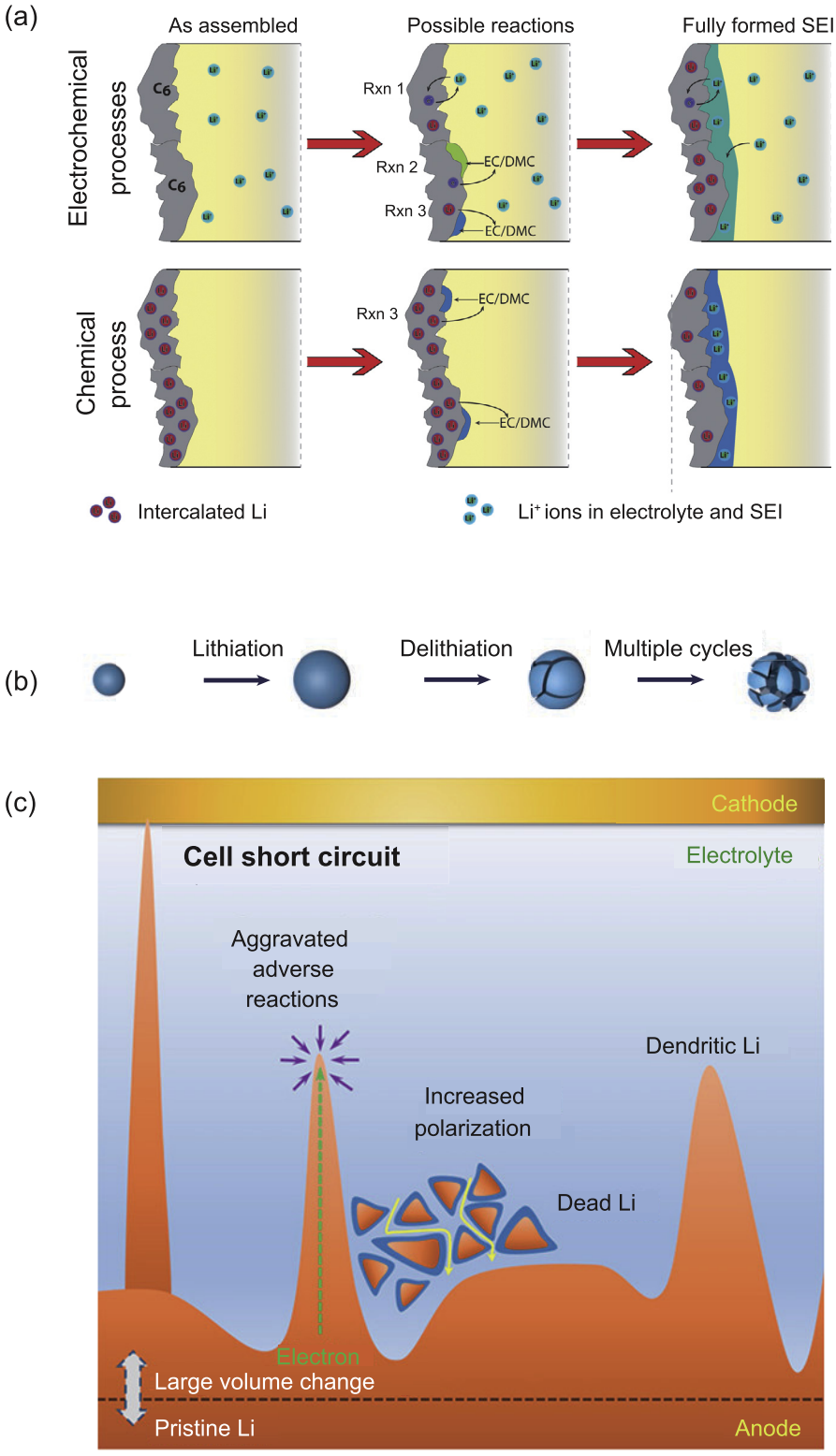

Fig. 2. Schematic of (a) loss of electrode materials, (b) structure deformation, and (c) dendrite growth on Li metal anode from Ref. [67] @ copyright 2015 American Chemical Society and Ref. [68] @ copyright 2017 American Chemical Society).

characterize the stress field and the evolution of the stress in the anode. In these years, several investigations have been performed to provide essential data to analyze failure mechanisms of the graphite anode.

$$a\text{-}C \overset{Li}{\leftrightarrow} a\text{-}Li_{0.5}C \quad (2)$$

Equation (2) indicates the change of phase structure in the graphite anode, which "a" represents the amorphous phase. This type of change is related to the anode failure.

Sethuraman et al. [78] measured stress changes in graphite anode by detecting the curvature changes of the substrate which was bonded to the graphite anode with an epoxy layer during electrochemical cycling. They developed the multi-beam optical sensor (MOS) system to measure this curvature. The compressive stress increases during electrochemical intercalation, which reaches a maximum of 10–12 MPa. It is indicated that an approximate correlation exists, which is between the rate of stress increase and the lithiated behavior of the graphite anode. Meanwhile, they have demonstrated that this method has the potential to be used to assess the mechanical performance of the anode material and capacity fading of the anode after cycling repeatedly. Furthermore, this technique is expected to serve as an effective tool to detect stress evolution in other anode materials upon lithiation.

To investigate the relationship between strains and anode failure, Jones et al. [61] utilized digital image correlation (DIC) to measure the strains that generate in the graphite anode during the process of electrochemical cycling. The experimental configuration consists of the camera, zoom lens, laser, and custom battery cell during electrochemical cycling. The camera is used for imaging device of conventional battery cell during electrochemical cycling. The fluorescent speckle pattern on the electrode surface is excited by a 532 nm laser. Reflected laser light is filtered to ensure that only the fluorescent emitted light can be captured in the images. Free-standing, unconstrained graphite anodes were cycled in the custom battery cells that provide optical access to the anodes during cycling. Speckle patterns for digital image correlation were generated by using fluorescent silica nanoparticles. In-house DIC code was used to correlate images that were captured to calculate *in situ* strains which developed in the graphite anode. Experimental results indicate that the volume of the graphite anode expands 1.41% and contracts 1.33% during electrochemical cycling. With a further study of the relationship between anode mechanical properties and battery performance, new designed anode can be engineered to improve the capacity and durability of lithium-ion batteries.

It is known that anode failure induced by volume change is closely linked with mechanical properties. To investigate the chemomechanical response of graphite anode, Tavassol et al. [79] defined the electrochemical stiffness (k), which represents the ratio of $\partial(\Delta\sigma)$ and $\partial(\varepsilon)$. $\partial(\Delta\sigma)$ is generated by the lithiation of the constrained anode compared with the corresponding incremental change in strain. $\partial(\varepsilon)$ is caused by the same lithiation in the unconstrained anode:

$$k_i = \frac{(-\Delta\sigma)}{\partial\varepsilon}\Big|_i \quad (3)$$

where i is either the electrode potential, E, or the electrode capacity, Q. They developed this novel method to attain the electrochemical stiffness by *in situ* stress and strain measurements and calculations.

In Fig. 3a–b, the methodology is illustrated to link stress and strain measurements to calculate the electrochemical stiffness of graphite anode. The electrode potential is the independent variable in the cyclic voltammetry, the potential-dependent stiffness (k_E) is calculated. During the process of galvanostatic cycling, the capacity-dependent stiffness (k_Q) is calculated, where electrode capacity is the independent variable. Therefore, these values of the electrochemical stiffness are obtained by measuring the relative effects of stress compared with strain during cycling, which is different from the conventional definition of stiffness. The potential-dependent variations in stiffness are caused by asynchronous rate of stress and strain (Fig. 3c). The asynchronous change of stress and strain shown in Fig. 3c indicates that the responses of the stress and strain in graphite anodes are the results of different potential-dependent phenomena. Schematic of the proposed driving forces of stress and strain development is presented in Fig. 3d. The stress is considered to be closely related to the surface charge, and it is assumed that this increase of stress before the transition is induced by concentration gradients in lithium-ion, due to the limited surface diffusion of lithium-ion through the graphite anodes. Impedance studies on graphite anodes indicate a sharp change in the lithium-ion diffusion coefficients during the phase transitions. Meanwhile, Li diffusion constant decreases greatly which occurs before the diluting stage I to stage IV transition. This decrease is consistent with the large change in stress (Fig. 3c). Electrochemical stiffness changes dramatically due to the process of lithium ion intercalation during cycling. These results reveal that stress depends proportionally on the rate of lithiation/delithiation and strain depends proportionally on the capacity. This electrochemical stiffness can be utilized to design novel anode materials for lithium-ion battery.

These measurements and analyses indicate that stress and strain developed in the graphite can result in the volume change of anode material. This volume change is much less than that of silicon anode. Graphite is widely used as the anode material of lithium-ion battery due to structural stability, but the capacity of graphite anode cannot meet the increasing demand of lithium-ion battery.

2.2.2. Silicon anode

Silicon is considered to be a promising anode material to improve battery performance. Silicon anode materials mainly consist of silicon nanowires, silicon nanospheres, silicon nanoparticles, and silicon thin films [19,32,80–87]. The capacity of silicon anode is much higher than that of graphite. However, it is a major issue that silicon experiences large volume changes during cycling, which leads to capacity fading, fracture and failure of battery [88–90]. In these years, a

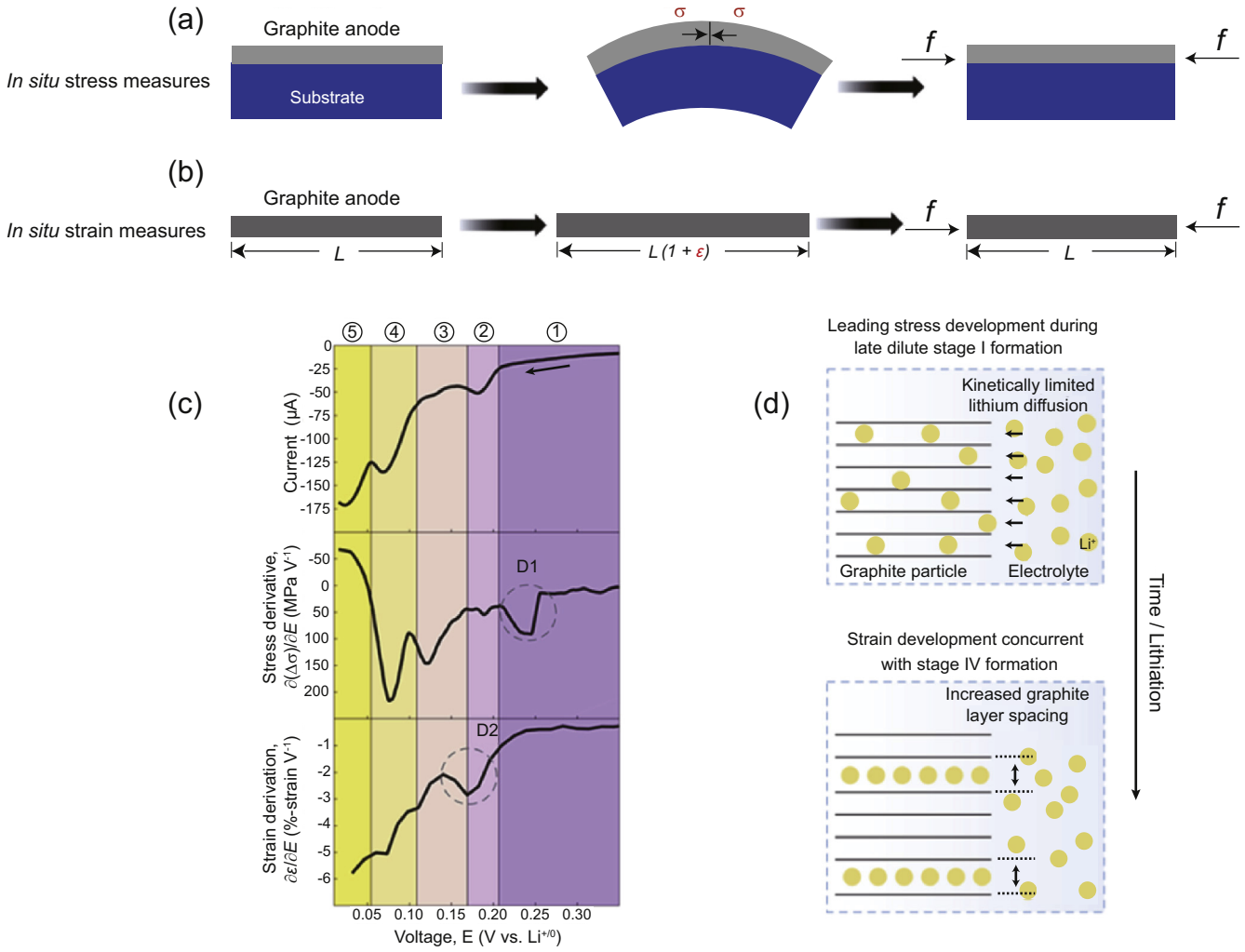

Fig. 3. Schematic illustration of electrochemical stiffness in lithium-ion batteries (reprinted with permission from Ref. [79] @ copyright 2016 Nature Publishing Group).

great deal of research about failure mechanisms of silicon anode material has been carried out to improve battery performance [77,91–94].

It is of significant importance that a deep understanding of the structural instability of silicon anodes during cycling could provide the solutions to retard the mechanical failure. *In situ* detection techniques have been used in the investigations of silicon anode failure, which can track the structural evolution of silicon anodes during cycling. *In situ* transmission electron microscopy (TEM) was used as a critical tool to carry out real time and atomic scale observations of the silicon anode by Liu et al. [62] during charging and discharging processes, which can be used to investigate the fracture process of silicon anode material in the lithium-ion battery. The fracture of Si particle with a diameter of 540 nm during lithiation was shown in Fig. 4a. The round initial Si particle changed to be polyhedral gradually during the lithiation process. It is indicated that the lithiation process was anisotropic, because some collisions can be seen on particle surfaces (Fig. 4b–d). When the diameter of lithiated particle changed into 200 nm, cracks were gradually initiated from these particle surfaces (Fig. 4e–g). These cracks developed and finally caused the fracture of the silicon anode after lithiation repeatedly. *In situ* TEM is also used by McDowell et al. [95] to observe the process of lithiation/delithiation of amorphous silicon(α-Si) nanospheres, which can reveal the fracture process of Si anode material.

Another investigation was carried out by *in situ* TEM. The *in situ* TEM cell was shown in Fig. 5a. With these a-Si spheres being dispersed, the Si pillar arrays have been etched into the Si wafer, and the Si wafer is attached to the copper rod. Li metal is selected as the counter electrode, which is coated with a thin Li_2O on the tip of the tungsten rod as the solid electrolyte interphase layer. TEM images of the lithiation process of the a-Si sphere were listed in Fig. 5b–e. Before the process of lithiation, the diameter of the a-Si sphere was 569 nm. While it became 792 nm after lithiation, indicating the volume expansion of the silicon anode is about 170%. Synthesizing the other 25 a-Si spheres that were measured and calculated, the volume expansion ranged from 101% to 332%, reaching the average of 204%. This variety of volume expansion is

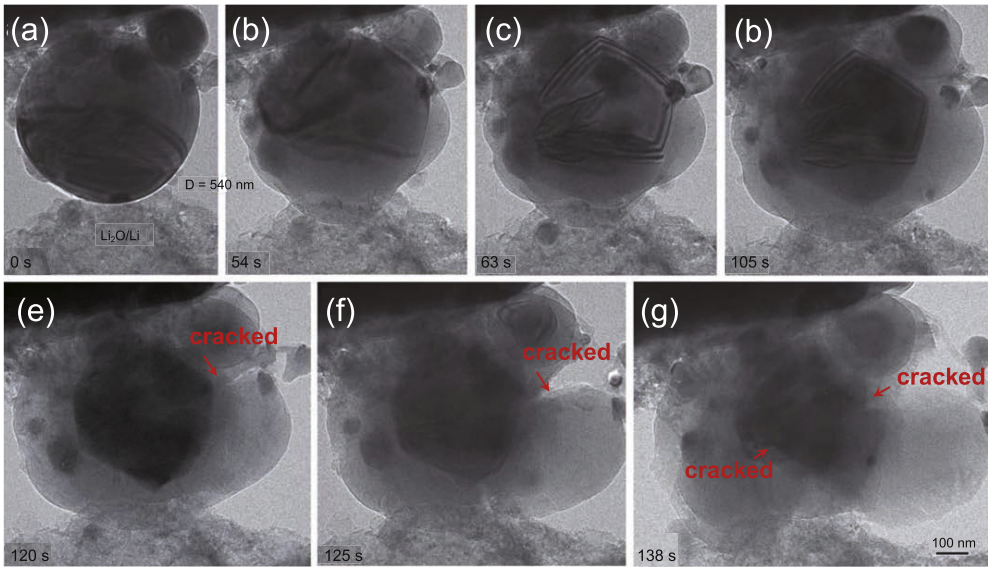

Fig. 4. (a) Schematic illustration of *in situ* TEM experiments, (b)–(e) Bright-field TEM images of the lithiation process of the a-Si sphere (reprinted with permission from Ref. [95] @ copyright 2013 American Chemical Society).

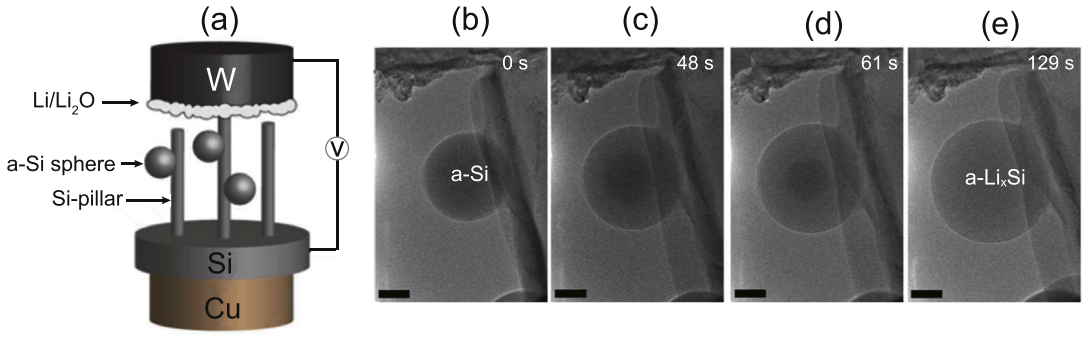

Fig. 5. Fracture process of Si anode material by *in situ* TEM (reprinted with permission from Ref. [62] @ copyright 2011 Royal Chemical Society).

mainly caused by different experimental conditions, such as the thickness of the solid electrolyte interphase layer or the quality of electrical contact. These factors generate different degrees of lithiation in the silicon anode. Unexpectedly, the results of the experiments also indicate that the first lithiation occurs by a two-phase mechanism, the darker phase is the Si-rich core and the lighter one is Li-rich shell. The results have an important influence on the evolution of mechanical stress. Based on the kinetics measurements, this behavior is due to the Si–Si bond breaking [96,97]. From the results, it is shown that amorphous Si has better performance on resisting fracture than crystalline Si when reacting with Li, which is advantageous to be utilized in the anode of the lithium-ion battery.

Zeng et al. [98] used *in situ* Raman spectroscopy to investigate stress in silicon anodes induced by lithiation. A tensile stress of 0.2 GPa was observed in silicon anodes when lithiated initially, then the compressive stress increased up to 0.3 GPa upon when lithiated gradually. Raman spectra of silicon in the battery during lithiation was shown in Fig. 6a. In the first 4 h, the intensity of silicon Raman peak stays comparatively high, but an apparent decrease was followed when lithiated gradually, which is consistent with the electrochemical reaction of silicon anodes. The lithiation of silicon initiates at about 4 h, the outer layer of silicon has changed into α-Li_xSi ($x = 3.4 \pm 2$), which has a much higher conductivity than silicon [99]. The high conductivity of α-Li_xSi means a small penetration depth of the laser, which will lead to the decrease of silicon peak intensity. Meanwhile, the intensity of the Raman peaks of the electrolyte remains almost invariant, which indicates that this change of silicon Raman peak is related to the electrochemical reaction. It can be seen from Fig. 6b–d that the peak position (X_c), full-width at half-maximum (FWHM) of the peak and adjusted R^2 value changed with the lithiation time. During the first 2 h, the Raman peak shifts to lower wavenumber, and then after 4 h, it shifts to higher wavenumber when lithiated gradually. The FWHM of the peak increases along with the lithiation process, which could lead to the stress induced lattice distortion. It is also shown that an increasing compressive stress developed in the silicon core during lithiation process. The compression of silicon core induced a tensile stress in the α-Li_xSi shell, which is likely to form cracks. Moreover, it is observed that the stress

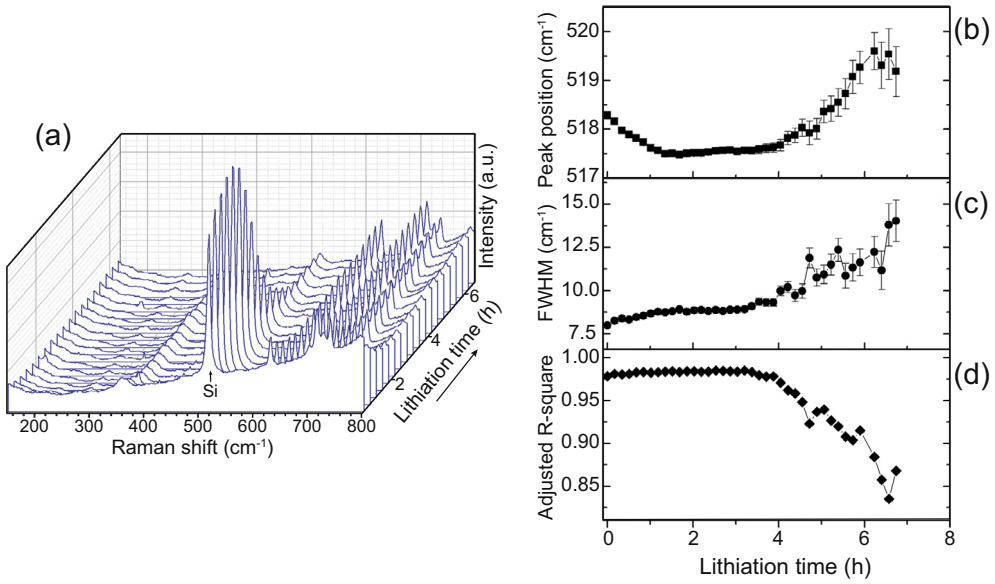

Fig. 6. (a) Selected Raman spectra, (b) the peak position, (c) full-width at half-maximum (FWHM) of the peak, (d) Adjusted R^2 during lithiation (reprinted with permission from Ref. [98] @ copyright 2016 Elsevier).

in the silicon core changed from tension to compression when lithiated gradually. Therefore, these experimental results provide the first quantitative data of stress in silicon anodes during lithiation process, which will improve the failure mechanisms of silicon anodes.

As reported by Duay et al. [100], they developed the *in situ* spectroelectrochemical optical diffraction (high-resolution) to investigate the process of volume change of the silicon anode. Teflon cell was assembled in the glovebox. The optical microscope is used to monitor of the diffraction efficiency of gratings during the process of lithiation and delithiation. Compared with TEM in terms of observing silicon's volume expansion, this method can provide better real-time monitoring of the volume change during the process of charge/discharge. During cycling, the volume change of silicon thin-film gratings has been characterized using the *in situ* optical diffraction to attain two essential items. One is the lateral expansion requiring the synthesis of silicon to be performed on opaque Pyrolyzed Photoresist Film (PPF) gratings, the other is the thickness changes requiring silicon to be synthesized on transparent PPF gratings. It could be found that the change of thickness was calculated for the 10th cycle. The thickness value increases with the growth of the wavelength. When the wavelength is 475 nm, a maximum increase has reached at 22.8 nm. While the wavelength reaches at 630 nm, the maximum increase of 29.6 nm can be acquired. The calculated thickness does not increase when the lithiation current is below 0.51 V. Moreover, the thickness continuously increases even after the voltage sweep changes from cathodic to anodic. This increase in the thickness continues increasingly until the current changes anodic at around 0.51 V. Then the silicon anode contracts back to its initial thickness when potentials are above 0.51 V. It can be concluded that the silicon's volume expands at potentials below 0.51 V during cyclic voltammetry, and contracts when potentials are above 0.51 V, which is independent of the sweep direction. *In situ* optical diffraction approach is a promising method to observe volume change of silicon anode beyond the first few cycles in a genuine battery environment. These promising results provide a new insight into figuring out the failure mechanisms of silicon anodes in lithium-ion batteries.

Bordes et al. [101] developed an innovative approach by using *in situ* focused ion beam to investigate silicon reaction mechanisms, which was implemented by means of the analysis chamber of a state-of-the-art time of flight secondary ion mass spectrometer. Detailed mapping of elements distribution can be performed. Core-shell mechanism and evolution was examined during the first cycle. This mechanism was observed for all particles in the silicon anodes, which had nothing to do with the position of these particles. Auger spectroscopy was performed to quantify the concentration of lithium in the entire shell. Meanwhile, the paths that lithium trapped into the silicon core could be observed by SEM and TEM. This method provided evidence of lithium getting through silicon particles after aging, which is related to capacity loss during long-life cycling.

In these years, some other silicon-based anodes with high capacity have attracted a lot of attention. SiO anode was proved to be a better choice. The theoretical reversible capacity of this anode is over 1710 mA h g^{-1} (based on reaction 4 and 5) [102]. More importantly, SiO has a smaller volume expansion than that of Si.

$$\mathrm{SiO} \xrightarrow{\mathrm{Li}} \frac{1}{4}\mathrm{SiO} + \frac{3}{4}\mathrm{Si} \quad \text{(irreversible)} \tag{4}$$

$$\frac{1}{4}\mathrm{Li_4SiO_4} + \frac{3}{4}\mathrm{Si} \xrightarrow{\mathrm{Li}} \frac{1}{4}\mathrm{Li_4SiO_4} + \frac{3}{4}\mathrm{Li_{15}Si_4}\text{(reversible)} \tag{5}$$

Kim et al. [103] investigated the lithiation mechanism in SiO as the anode of lithium-ion batteries. In this research, the microstructure and electrochemical performance of SiO were investigated using solid-state NMR and electrochemical dilatometry technique. They also observed the formation of crack at the two-phase boundaries and the pulverization, which indicated the initial volume expansion of 132% and a reversible volume expansion of 117%. Overall, SiO is a great candidate for the high energy density coin cells, and it is worth expecting to apply SiO into the realistic industry of lithium-ion battery.

2.2.3. Lithium metal anode

Lithium metal has a high theoretical capacity (3860 mA h g^{-1}), but it suffers from poor rechargeability and low safety. The reductive decomposition and the corrosion of the lithium metal anode would cause the formation of SEI layer, which would lead to the decrease of irreversible lithium and the degradation and failure of anode material [104]. However, lithium dendrite formation is the main reason of lithium metal anode failure, which leads to puncture the separator and consequently initiates internal short circuits [105–109]. It is difficult to detect lithium dendrite since it can be decomposed by surge currents of internal short circuit.

In situ optical microscopy is an effective method to observe the lithium dendrite growth process, which can easily and instantaneously identify the dendrite formation and the change of anode surface. Brissot et al. [110] used this method to study lithium dendrite growth in lithium/PEO-salt/lithium cells. They developed a novel optical cell, which could work as an air-tight electrochemical cell. The observations indicated that the growth rate of the dendrites seems to get close to the theoretical value of the velocity. Meanwhile, they proved that the movement of this electrolyte could disconnect dendrites from the lithium anode.

Huang et al. [111] used *in situ* TEM to observe the lithium dendrite growth on anodes for lithium-ion batteries. They found that lithium dendrite with a length of 35 μm grew on the anode during charging. This study also reveals a potential safety concern of short-circuit failure for lithium-ion batteries. *In situ* TEM was also used by Yassar et al. to investigate the growth of lithium dendrites [112]. They observed the nucleation of lithium ions at the anode/electrolyte interphase and the lithium dendrites growth on the anode surface.

Cryo-electron microscopy (cryo-EM) is an effective tool to observe the beam-sensitive lithium dendrite. Cui et al. observed the growth of lithium dendrites in carbonate-based electrolytes using cryo-transmission electron microscopy (cryo-TEM) [113]. Cryo-TEM enables to preserve the native state of chemically reactive and beam-sensitive battery materials after operation, which presents a simple methodology to preserve and image sensitive battery materials with atomic resolution, revealing detailed nanostructures. Kourkoutis et al. [114] established a method that used cryo-TEM to observe the solid–liquid interfaces of lithium anode, by vitrifying the liquid electrolyte and hence preserving the structures at their native state. They identified two dendrite types coexisting on the lithium anode, each with distinct structure and composition. This research provided a new insight into the formation of lithium dendrites, which demonstrated the potential of cryo-EM for probing nanoscale processes at intact solid–liquid interfaces in rechargeable batteries. Meng et al. [115]developed an analytical method of titration gas chromatography to quantify the contribution of unreacted (dead) metallic Li^0 to the total amount of inactive lithium. They identified the dead metallic Li^0, not the electrochemically formed Li^+ in the SEI layer, leading to the dominant source of inactive lithium and capacity loss. By coupling the unreacted metallic Li^0 content to observations of its local microstructure and nanostructure by cryo-EM(both scanning and transmission), they also established the formation mechanism of inactive lithium in different types of electrolytes and determined the underlying cause of low Coulombic efficiency in the charging and discharging process for lithium metal anode.

2.3. Discussion of different techniques to investigate anode failure

Anode material is a crucial part of lithium-ion battery. The anode failure restricts the electrochemical performance and cycle life. Therefore, it is of great importance to investigate the failure mechanism of the anode material. Herein, we summarized the recent advances of different anode failure mechanisms attained by using various methods (Table 2). In this table, we summarized the failure investigations of different anode materials, including graphite, silicon, tin, lithium metal, and some other composited materials. It is indicated that we need to pay more attention to carry out research about failure mechanisms of some promising anode with high capacity and efficiency, such as tin and silicon. It is conducive to innovate the anode material, and also predestined to promote the industry of lithium-ion battery.

Meantime, *in situ* techniques and other advanced methods have been developed to investigate the anode failure, which show different characteristic. Some methods (multi-beam optical sensor system, digital image correlation system, *in situ* AFM, *in situ* Raman spectroscopy, *in situ* stress and strain measurements) can quantify the mechanical properties of the anodes during electrochemical cycling, including stress, strain, and Young's modulus. These mechanical parameters can describe the evolution process of anode failure. Several methods including *in situ* TEM and *in situ* NMR can be used to observe the formation of lithium dendrites and provide direct evidence of the atomic scale when cycling.

It is a general trend to apply *in situ* detection techniques to reveal anode failure mechanisms. Meanwhile, it is promising to combine measures of mechanics properties with *in situ* techniques recently and progress on *in situ* observation will be highly promoted in the future. This insight allows the nature of structural change to be revealed. With a better understanding of the failure mechanisms, novel stable structures and

Table 2
Summary of different failure phenomena for anode materials in lithium-ion batteries.

Anode materials	Material types	Methodologies	Expansion (%)	Remarks	Ref.
C	Graphite particle	Multi-beam optical sensor system	–	Describe the nature of stress evolution in graphite anodes and provide crucial data to quantify the driving force which leads to mechanical failure	[78]
C	Graphite particle	Digital image correlation system	1.41	Quantify the strain generated in the anodes of lithium-ion battery during cycling.	[61]
C	Graphite particle	*In situ* stress and strain measurements	–	Reveal the dramatic changes in electrochemical stiffness due to the various intercalation compounds formed during cycling	[79]
Si	Nano particle	*In situ* TEM	101–332	Direct evidence of lithiation mechanism of silicon anode at the atomic scale	[62,95]
Si	Nano wire	*In situ* AFM	–	Track the morphology and Young's modulus of the individual silicon anode surface quantitatively during the SEI growth	[116]
Si	Nano particle	*In situ* Raman spectroscopy	–	Provide the first quantitative experimental data of stress in nanostructured silicon anodes during lithiation	[98]
Si	Thin film	*In situ* spectroelectrochemical optical diffraction	–	A novel and relatively inexpensive way of obtaining the volume change of silicon anode beyond the first cycles of silicon thin films in the practical battery environment	[100]
Si	Nanowire	*In situ* NMR	–	Anode structure investigation at an atomistic level for multiple cycles	[117]
Si	Micro particle	Time-of-flight secondary ion mass spectrometer	–	Reveal the lithiation mechanisms of silicon anode during the first cycle	[101]
SiO	Micro particle	Solid-state NMR and TEM	117	Observe the formation of the crack at the two-phase boundaries	[103]
Li	Lithium metal	*In situ* TEM	–	Observe the nucleation of lithium ions at the anode/electrolyte interphase and the lithium dendrites growth on the anode surface	[112]
Li	Lithium metal	Cryo-EM	–	Observe the beam-sensitive lithium dendrite	[114]
Li	Lithium metal	Titration gas chromatography	–	Quantify the contribution of unreacted (dead) metallic Li^0 to the total amount of inactive lithium	[115]

materials have been developed to improve the performance and extend the cycle life.

3. Suppression of anode internal failure

The investigation of the anode failure mechanism is considered as a foundation for more robust and durable anodes for next-generation lithium-ion battery. Based on the analysis of anode failure mechanisms, novel methods and materials have been designed to enhance the fracture resistance of the anode material [118–124]. For some repairable anode failure, new methods can heal the cracks to extend the cycle life. However, some anode materials need novel structures to resist tremendous volume changes.

3.1. Graphite anode

During the charge and discharge process, SEI layer formation is one of the most important processes significantly affecting the Coulombic efficiency and even cycle life. SEI layer formation on the surface of graphite anode causes loss of lithium. The existence of oxygen groups on graphite anode surface contributes to SEI formation. Modification of graphite surface was introduced to suppress this failure.

Heat treatment in oxygen or argon is a typical method to control oxygen levels on graphite anode surface to introduce or remove oxygen groups [125]. Meanwhile, An et al. [126]introduced UV light into graphite anode of lithium-ion battery to control oxygen levels on the graphite anode to extend battery cycle life. They treated graphite powder under UV light, and it showed that UV light with humid air increased oxygen levels, particularly in hydroxyl form, on graphite surfaces. It was found that UV treatment of the anode resulted in thinner SEI layers, higher capacity retentions, and lower charge transfer resistance after cycling. XPS results indicated that three times increase in atomic percentage of oxygen occurred on the graphite powder surfaces after UV treatment, which suppressed the SEI formation and improved the cycling stability of lithium-ion batteries.

3.2. Silicon-based anode

On the basis of graphite anode failure mechanisms, electrolyte additives are considered as a promising choice to prevent anode from fracture and failure. Electrolyte additives can change the SEI layer, improve the mechanical properties of this cohesive layer and contribute to suppressing the anode fracture. The performance of silicon anode was investigated with the anode SEI forming additives existed. Dalavi et al. [127] added vinylene carbonate, fluoroethylene carbonate, and lithium difluorooxalatoborate into $LiPF_6$ electrolytes, which improved the fracture resistance of the silicon thin film anode effectively. As a result, these electrolyte additives promote the capacity and cycling performance of the batteries. Meantime, novel binders have been developed to accommodate the large volume change of anodes. Song et al. [128] created a type of interpenetrated gel polymer binder to extend the lifetime of Si anode through *in situ* crosslinking of water soluble poly (acrylic acid) (PAA) and polyvinyl alcohol (PVA) precursors. Excellent cycling stability and high Coulombic efficiency even at high current densities can be obtained using this binder.

The formation of stable Si anodes is a challenge because of significant volume changes occurring during their electrochemical alloying and dealloying with Li. Binder selection and optimization may allow significant improvements in the stability of Si-based anodes. Most studies of Si anodes have involved the use of carboxymethylcellulose (CMC) and poly(vinylidene fluoride) (PVDF) binders. Herein, we show for the first time that pure poly(acrylic acid) (PAA), possessing certain mechanical properties comparable to those of CMC but containing a higher concentration of carboxylic functional groups, may offer superior performance as a binder for Si anodes. We further show the positive impact of carbon coating on the stability of the anode. The carbon-coated Si nanopowder anodes, tested between 0.01 and 1 V vs. Li/Li^+ and containing as little as 15 wt% of PAA, showed excellent stability during the first hundred cycles. The results obtained open new avenues to explore a novel series of binders from the polyvinyl acids (PVA) family. Wang et al. reported an interpenetrated gel polymer binder for high-performance silicon anodes, which were prepared by *in situ* crosslinking of water-soluble poly(acrylic acid) (PAA) and polyvinyl alcohol (PVA) precursors. This gel polymer binder with deformable polymer network and strong adhesion on silicon particles can effectively accommodate the large volume change of silicon anodes upon lithiation/delithiation, leading to an excellent cycling stability and high Coulombic efficiency even at high current densities.

Nanocomposites with various carbon matrices have been designed to resist the tremendous volume change of silicon anode materials, which extend the cycle life of lithium-ion batteries. Cracks can be repaired by means of electrolyte additives, and large volume changes are accommodated by various novel structures and materials. All these methods of resisting anode failure are conductive to extend the cycle life of lithium-ion batteries. Next challenge that we faced with is how to reduce the cost of these promising anode materials, which may contribute to the lithium-ion battery industry.

Silicon-carbon composited anode has become a promising method to prevent the volume change of anode material. Yushin's group developed a method to design the nanocomposite particles, which offered potential in energy-storage application [129].

$$\text{Carbon black} \rightarrow \text{Si CVD} \rightarrow \text{C CVD Spherical granules} \quad (6)$$

Equation (6) shows the synthesis process of this anode material. The synthesis method of chemical vapour deposition (CVD) is designed to attain the carbon-black nanoparticles coated by silicon nanoparticles, which branched into short chains during the process of high-temperature pre-annealing. Subsequently, the 0.5–1 μm multi-branched nanocomposite is self-assembled into the spherical particles with large porosity during the CVD deposition of C at the atmospheric pressure (Fig. 7a). This robust sphere structure with irregular channels provided rapid access of lithium-ion into the particle. Meanwhile, large volume changes of silicon anode during the lithiation and delithiation are accommodated by the internal porosity of the particles. High reversible capacity (1950 mA h g^{-1}) and stable performance can be obtained. Moreover, this synthesis method is simple, safe, inexpensive and widely applicable, which provides a novel engineering-oriented path of anode materials with better performance.

Graphite oxide (GO) and reduced graphite oxide (RGO) have been used to resist the large volume change of silicon

Fig. 7. (a) Schematic of Si–C nanocomposite particle formation through hierarchical bottom-up assembly (reprinted with permission from Ref. [129] @ copyright 2010 Nature Publishing Group), (b) Schematic of the pomegranate-inspired design of silicon anode (reprinted with permission from Ref. [130] @ copyright 2014 Nature Publishing Group), (c) Schematic illustration of the packing model for Si/C anodes (reprinted with permission from Ref. [131] @ copyright 2016 Wiley).

anode. Wang et al. [119] developed a new type of self-supporting binder-free silicon-based anode, which is encapsulated by silicon nanowires (SiNWs) with dual layers of an overlapping graphene sheath. This structure can prevent the direct exposure of encapsulated silicon to the electrolyte and enable the structural and interfacial stabilization of silicon nanowires. Meanwhile, this type of anode can accommodate the volume change and maintain the structural stability, which also exhibits high reversible capacity and great cycling performance.

Interestingly, investigation inspired by living organisms in nature was reported to overcome the fracture and failure of the anode materials. Inspired by the structure of pomegranate, Cui's group [130] reported a novel silicon anode encapsulated by a conductive carbon layer (Fig. 7b).

$$\text{Si nanoparticle} \rightarrow \text{Si@SiO}_2 \rightarrow \text{Microemulsion droplet} \rightarrow \text{Si@SiO}_2\text{cluster} \rightarrow \text{Si@SiO}_2\text{@C cluster} \rightarrow \text{Si pomegranate} \quad (7)$$

The synthesis process of this silicon anode was shown in the equation (7). This method can retain enough space for expansion and contraction during cycling. The silicon nanoparticles are encapsulated by carbon layer in pouches to be used as an electrolyte barrier. The SEI layer remains stable and spatially confined, leading to superior cycle performance, which can retain 97% capacity after 1,000 cycles. This microstructure decreases the contact area between the silicon anode and electrolyte effectively, which results in high Coulombic efficiency (99.87%). Meanwhile, after 100 cycles, it is observed that the thin and uniform SEI coating is encapsulated the silicon anode. When the SEI was removed with acid, entire carbon shells can be seen clearly. They analyzed and compared the diameter of the silicon pomegranates, which indicates only a 10% increase. In this study, the volumetric change of the anode is much less than that of common silicon anode, and it is extremely crucial for excellent performance in new type anodes of the lithium-ion batteries.

Watermelon can inspire researchers to investigate the anode materials. Guo's group [131] designed and synthesized the watermelon-inspired silicon-carbon microspheres, which can alleviate the volumetric change and anode fracture under a high pressing density. The advantages of this novel design (Fig. 7c) can be summarized in the following aspects. The silicon nanoparticles (< 100 nm) can effectively resist the pulverization of silicon, and silicon nanoparticles which are coated by graphite can relieve the large volumetric change of Si during cycling. The volume expansion of silicon can be accommodated in the internal void space. It is revealed that this optimized size distribution is conducive to achieve efficient utilization of space. Considering the practical application, this Si/C anode presents the appropriate capacity (620 mA h g^{-1}). Furthermore, the superior initial Coulombic efficiency (89.2%) and average Coulombic efficiency (99.8%) can be achieved.

3.3. Lithium metal anode

Dendrite growth on lithium metal anode causes capacity loss and short circuit, which are major barriers to next-generation batteries. Novel separator, addictive could provide new insights to mitigate the formation lithium metal dendrite.

Wu et al. [132] reported a multifunctional separator based on layer-by-layer self-assembly of 2D MoS_2 nanomaterials which contributed to the suppression of lithium dendrite growth, benefiting from the high mechanical modulus that physically restrained the dendrite growth, and the accelerated lithium-ion diffusion that regulated lithium-ion deposition on the lithium anode.

Goodenough et al. [133] developed a lithium metal anode that was fabricated with a low cost and was stable in air. They eliminated the liquid-electrolyte ethylene-carbonate additive to *in situ* form a SEI passivation layer on the lithium metal anode, which suppressed the Li dendrite growth during long-term cycling.

Wang et al. [134] demonstrated the enabling role of plating residual stress in dendrite formation through depositing lithium on soft substrates and a stress-driven dendrite growth model. They revealed that dendrite growth was mitigated on such soft substrates through surface-wrinkling-induced stress relaxation in the deposited lithium film. Meanwhile, they demonstrated that this dendrite mitigation mechanism could be applied synergistically with other existing methods in the form of three-dimensional soft scaffolds for lithium plating. It can achieve higher Coulombic efficiency and excellent capacity retention than that for typical copper substrates.

4. Summary and outlook

Nowadays, our life is being changed due to the appearance of the lithium-ion battery [135]. As a vital part of the electrodes, the anode material performance is of significant importance for the research and development of advanced lithium-ion batteries [136–139]. The anode failure restricts the electrochemical performance and cycle life. The internal failure of the anode material is worth being investigated [31,40,140,141].

From the material science aspect, (1) the SEI formation roots in the irreversible chemical reactions of electrolytes with the anode materials; (2)The structure deformation results from the crystal structure change upon the uptake of Li-ions. The volume variation appears to be more pronounced for higher capacity materials (e.g. Si and Li). The so-called zero-strain materials (e.g. $Li_4Ti_5O_{12}$) exhibits lower capacity but greatly stable structure over cycling as they undergoes less than 0.5% of volume expansion upon lithium-ion insertion. (3) The dendritic Li deposition is caused by the non-homogeneous charge distribution. It is unavoidable, and can only be suppressed to some extent with proper approaches to obtain sustained cycle life.

In situ and *operando* X-ray, microscopy and spectroscopic techniques have been intensively researched for the diagnosis of battery failures, providing detailed and comprehensive information about the crystallographic, morphological and chemical evolutions. However, these studies often only investigate into the failures with individual single techniques. Versatile characterization platforms combining multiple advanced techniques may be an effective solution to monitor the battery failure from various aspects and at multiple spatial dimensions. For instance, a combined XRD-optical microscopy station simutaneously probes the phase transformation and macroscale morphological evolution of anode materials. Meanwhile, these techniques can also be integrated with mechanical (e.g. Young's modulus) and thermal (e.g. temperature monitoring) methods for more effective and efficient failure detection.

Understanding the nature of anode failure is possible to provide guidance to optimize surface modification and anode material development to increase the material ductility and resist the high surface stress. Suppression of anode failure is the primary requirement to extend the cycle life of the battery from a practical application point of view. Subsequently, novel stable structures and materials have been developed to improve the performance and extend the cycle life [142]. These designs effectively enhanced the resistibility to volume changes of anode materials. Cracks and lithium dendrite can be suppressed by adding additives into the electrolyte, and large volume changes are accommodated by various novel structures and materials. It is believed that better understanding of the anode failure mechanisms could contribute to the development of anode material design and main strategies towards the advances in durable anodes of lithium-ion batteries.

Declaration of competing interest

We declare that we have no financial and personal relationships with other people or organizations that can inappropriately influence our work, there is no professional or other personal interest of any nature or kind in any product, service and/or company that could be construed as influencing the position presented in, or the review of the manuscript entitled.

Acknowledgement

The authors acknowledge the financial support on this research from National Key Research and Development Program of China (2017YFB0403300/2017YFB043305), National Natural Science Foundation of China under Grant No. 51425405, Key Program of Chinese Academy of Sciences KFZD-SW-315, and 1000 Talents Program of China (Z.S.).

References

[1] J.M. Tarascon, M. Armand, Nature 414 (2001) 359–367.
[2] M. Armand, J.M. Tarascon, Nature 451 (2008) 652–657.
[3] J.B. Goodenough, K.S. Park, J. Am. Chem. Soc. 135 (2013) 1167–1176.
[4] Y. Sun, N. Liu, Y. Cui, Nature Energy 1 (2016) 16071.
[5] S.B. Schougaard, Science 353 (2016) 543–544.
[6] J. Lim, Y.Y. Li, D.H. Alsem, H. So, S.C. Lee, P. Bai, D.A. Cogswell, X.Z. Liu, N. Jin, Y.S. Yu, N.J. Salmon, D.A. Shapiro, M.Z. Bazant, T. Tyliszczak, W.C. Chueh, Science 353 (2016) 566–571.
[7] Y. Li, K. Yan, H.-W. Lee, Z. Lu, N. Liu, Y. Cui, Nature Energy 1 (2016) 15029.
[8] L. Ma, M. Nie, J. Xia, J.R. Dahn, J. Power Sources 327 (2016) 145–150.
[9] J.N. Weker, N. Liu, S. Misra, J.C. Andrews, Y. Cui, M.F. Toney, Energy Environ. Sci. 7 (2014) 2771–2777.
[10] H. Wu, G. Chan, J.W. Choi, I. Ryu, Y. Yao, M.T. McDowell, S.W. Lee, A. Jackson, Y. Yang, L. Hu, Y. Cui, Nat. Nanotechnol. 7 (2012) 310–315.
[11] X.H. Liu, J.W. Wang, S. Huang, F. Fan, X. Huang, Y. Liu, S. Krylyuk, J. Yoo, S.A. Dayeh, A.V. Davydov, S.X. Mao, S.T. Picraux, S. Zhang, J. Li, T. Zhu, J.Y. Huang, Nat. Nanotechnol. 7 (2012) 749–756.
[12] J.W. Choi, D. Aurbach, Nature Rev. Mater. 1 (2016) 16013.
[13] M.J. Chon, V.A. Sethuraman, A. McCormick, V. Srinivasan, P.R. Guduru, Phys. Rev. Lett. 107 (2011) 045503.
[14] J. Xu, B. Liu, D. Hu, Sci. Rep. 6 (2016) 21829.
[15] I. Kovalenko, B. Zdyrko, A. Magasinski, B. Hertzberg, Z. Milicev, R. Burtovyy, I. Luzinov, G. Yushin, Science 334 (2011) 75–79.
[16] Y. Zhang, H. Shi, D. Song, H. Zhang, X. Shi, L. Zhang, J. Power Sources 327 (2016) 38–43.
[17] C.K. Chan, H.L. Peng, G. Liu, K. McIlwrath, X.F. Zhang, R.A. Huggins, Y. Cui, Nat. Nanotechnol. 3 (2008) 31–35.
[18] A. Barré, B. Deguilhem, S. Grolleau, M. Gérard, F. Suard, D. Riu, J. Power Sources 241 (2013) 680–689.
[19] L.A. Berla, S.W. Lee, Y. Cui, W.D. Nix, J. Power Sources 273 (2015) 41–51.
[20] J. Cannarella, C.B. Arnold, J. Power Sources 269 (2014) 7–14.
[21] W.-J. Lai, M.Y. Ali, J. Pan, J. Power Sources 245 (2014) 609–623.
[22] L. Liang, F. Jiang, Y. Cao, G. Hu, K. Du, Z. Peng, J. Power Sources 328 (2016) 422–432.
[23] W. Xu, J. Wang, F. Ding, X. Chen, E. Nasybulin, Y. Zhang, J.-G. Zhang, Energy Environ. Sci. 7 (2014) 513–537.
[24] Z. Gong, Y. Yang, Energy Environ. Sci. 4 (2011) 3223–3242.
[25] V. Etacheri, R. Marom, R. Elazari, G. Salitra, D. Aurbach, Energy Environ. Sci. 4 (2011) 3243.
[26] H.C. Wu, Z.Z. Guo, H.P. Wen, M.H. Yang, J. Power Sources 146 (2005) 736–740.
[27] T. Utsunomiya, O. Hatozaki, N. Yoshimoto, M. Egashira, M. Morita, J. Power Sources 196 (2011) 8675–8682.
[28] J. Vetter, P. Novák, M.R. Wagner, C. Veit, K.C. Möller, J.O. Besenhard, M. Winter, M. Wohlfahrt-Mehrens, C. Vogler, A. Hammouche, J. Power Sources 147 (2005) 269–281.
[29] V. Agubra, J. Fergus, Materials 6 (2013) 1310–1325.
[30] S. Huang, F. Fan, J. Li, S. Zhang, T. Zhu, Acta Mater. 61 (2013) 4354–4364.
[31] Y. Yao, M.T. Mcdowell, I. Ryu, H. Wu, N. Liu, L. Hu, W.D. Nix, Y. Cui, Nano Lett. 11 (2011) 2949–2954.
[32] H. Wu, G. Chan, J.W. Choi, I. Ryu, Y. Yao, M.T. Mcdowell, S.W. Lee, A. Jackson, Y. Yang, L. Hu, Nat. Nanotechnol. 7 (2012) 310–315.
[33] J.R. Szczech, J. Song, Energy Environ. Sci. 4 (2010) 56–72.
[34] T. Song, J. Xia, J.H. Lee, H.L. Dong, M.S. Kwon, J.M. Choi, W. Jian, S.K. Doo, H. Chang, W.I. Park, Nano Lett. 10 (2010) 1710–1716.
[35] B. Li, X. Gao, J. Li, C. Yuan, Environ. Sci. Technol. 48 (2014) 3047–3055.
[36] U. Kasavajjula, C. Wang, A.J. Appleby, J. Power Sources 163 (2007) 1003–1039.
[37] J.L. Dong, H. Lee, M.H. Ryou, G.B. Han, J.N. Lee, J. Song, J. Choi, K.Y. Cho, M.L. Yong, J.K. Park, ACS Appl. Mater. Interfaces 5 (2013) 12005–12010.
[38] Y. Chen, M. Nie, B.L. Lucht, A. Saha, P.R. Guduru, A. Bose, ACS Appl. Mater. Interfaces 6 (2014) 4678–4683.

[39] C.K. Chan, H. Peng, G. Liu, K. Mcilwrath, X.F. Zhang, R.A. Huggins, Y.I. Cui, Nat. Nanotechnol. 3 (2008) 31–35.
[40] C.K. Chan, R.N. Patel, M.J. O'Connell, B.A. Korgel, Y. Cui, ACS Nano 4 (2010) 1443–1450.
[41] X. Zhou, L. Ma, J. Yang, B. Huang, Y. Zou, J. Tang, J. Xie, S. Wang, G. Chen, J. Electroanal. Chem. 698 (2013) 39–44.
[42] U. Tanaka, T. Sogabe, H. Sakagoshi, M. Ito, T. Tojo, Carbon 39 (2001) 931–936.
[43] E. Rodríguez, I. Cameán, R. García, A.B. García, Electrochim. Acta 56 (2011) 5090–5094.
[44] H. Li, R.Y. Tay, S.H. Tsang, W. Liu, E.H.T. Teo, Electrochim. Acta 166 (2015) 197–205.
[45] B. Duan, W. Wang, H. Zhao, A. Wang, M. Wang, K. Yuan, Z. Yu, Y. Yang, Electrochem. Commun. 2 (2013) A47–A51.
[46] S. Banerjee, G. Periyasamy, S.K. Pati, J. Mater. Chem. 2 (2014) 3856–3864.
[47] T. Zhang, L.J. Fu, J. Gao, Y.P. Wu, R. Holze, H.Q. Wu, J. Power Sources 174 (2007) 770–773.
[48] Y. Xu, Y. Zhu, Y. Liu, C. Wang, Adv. Energy Mater. 3 (2013) 128–133.
[49] Y. Xu, J. Guo, C. Wang, J. Mater. Chem. 22 (2012) 9562–9567.
[50] Z. Shen, Y. Hu, Y. Chen, X. Zhang, K. Wang, R. Chen, J. Power Sources 278 (2015) 660–667.
[51] L. Liu, F. Xie, L. Jing, T. Zhao, T. Li, B.G. Choi, J. Power Sources 321 (2016) 11–35.
[52] W. Choi, J.Y. Lee, B.H. Jung, S.L. Hong, J. Power Sources 136 (2004) 154–159.
[53] G. Zheng, S.W. Lee, Z. Liang, H.W. Lee, K. Yan, H. Yao, H. Wang, W. Li, S. Chu, Y. Cui, Nat. Nanotechnol. 9 (2014) 618–623.
[54] T. Zhang, N. Imanishi, Y. Shimonishi, A. Hirano, J. Xie, Y. Takeda, O. Yamamoto, N. Sammes, J. Electrochem. Soc. 157 (2010) A214–A218.
[55] C.-P. Yang, Y.-X. Yin, S.-F. Zhang, N.-W. Li, Y.-G. Guo, Nat. Commun. 6 (2015) 8058.
[56] W. Xu, J. Wang, F. Ding, X. Chen, E. Nasybulin, Y. Zhang, J.G. Zhang, Energy Environ. Sci. 7 (2013) 513–537.
[57] M.H. Ryou, M.L. Yong, Y. Lee, M. Winter, P. Bieker, Adv. Funct. Mater. 25 (2015) 834–841.
[58] Q.C. Liu, J.J. Xu, S. Yuan, Z.W. Chang, D. Xu, Y.B. Yin, L. Li, H.X. Zhong, Y.S. Jiang, J.M. Yan, Adv. Mater. 27 (2015) 5241–5247.
[59] A.C. Kozen, C.F. Lin, A.J. Pearse, M.A. Schroeder, X. Han, L. Hu, S.B. Lee, G.W. Rubloff, M. Noked, ACS Nano 9 (2015) 5884–5892.
[60] L.-F. Cui, L. Hu, H. Wu, J.W. Choi, Y. Cui, J. Electrochem. Soc. 158 (2011) A592–A596.
[61] E.M.C. Jones, M.N. Silberstein, S.R. White, N.R. Sottos, Exp. Mech. 54 (2014) 971–985.
[62] X.H. Liu, J.Y. Huang, Energy Environ. Sci. 4 (2011) 3844–3860.
[63] B. Koo, H. Kim, Y. Cho, K.T. Lee, N.S. Choi, J. Cho, Angew. Chem. 51 (2012) 8762–8767.
[64] M.T. McDowell, I. Ryu, S.W. Lee, C. Wang, W.D. Nix, Y. Cui, Adv. Mater. 24 (2012) 6034–6041.
[65] S. Misra, N. Liu, J. Nelson, S.S. Hong, Y. Cui, M.F. Toney, ACS Nano 6 (2012) 5465–5473.
[66] M. Marinaro, M. Weinberger, M. Wohlfahrt-Mehrens, Electrochim. Acta 206 (2016) 99–107.
[67] R.L. Sacci, J.L. Bañuelos, G.M. Veith, K.C. Littrell, Y.Q. Cheng, C.U. Wildgruber, L.L. Jones, A.J. Ramirez-Cuesta, G. Rother, N.J. Dudney, J. Phys. Chem. C 119 (2015) 9816–9823.
[68] X.-B. Cheng, R. Zhang, C.-Z. Zhao, Q. Zhang, Chem. Rev. 117 (2017) 10403–10473.
[69] A. Mukhopadhyay, A. Tokranov, K. Sena, X. Xiao, B.W. Sheldon, Carbon 49 (2011) 2742–2749.
[70] W.J. Zhang, J. Power Sources 196 (2011) 13–24.
[71] A. Mukhopadhyay, B.W. Sheldon, Prog. Mater. Sci. 63 (2014) 58–116.
[72] H. Kim, G. Jeong, Y.U. Kim, J.H. Kim, C.M. Park, H.J. Sohn, Chem. Soc. Rev. 42 (2013) 9011–9034.
[73] Z. Guo, C. Liu, B. Lu, J. Feng, Carbon 150 (2019) 32–42.
[74] P. Zhang, T. Yuan, Y. Pang, C. Peng, J. Yang, Z.-F. Ma, S. Zheng, J. Electrochem. Soc. 166 (2019) A5489–A5495.
[75] C. Chen, Y. Wei, Z. Zhao, Y. Zou, D. Luo, Electrochim. Acta 305 (2019) 65–71.
[76] N. Iqbal, S. Lee, J. Electrochem. Soc. 165 (2018) A1961–A1970.
[77] S.N.S. Hapuarachchi, Z. Sun, C. Yan, Adv. Sustain. Syst. 2 (2018) 1700182.
[78] V.A. Sethuraman, N. Van Winkle, D.P. Abraham, A.F. Bower, P.R. Guduru, J. Power Sources 206 (2012) 334–342.
[79] H. Tavassol, E.M.C. Jones, N.R. Sottos, A.A. Gewirth, Nat. Mater. 15 (2016) 1182–1187.
[80] M.T. Mcdowell, I. Ryu, S.W. Lee, C. Wang, W.D. Nix, Y. Cui, Adv. Mater. 24 (2012) 6034–6041.
[81] A. Magasinski, P. Dixon, B. Hertzberg, A. Kvit, J. Ayala, G. Yushin, Nat. Mater. 9 (2010) 353–358.
[82] N. Liu, W. Hui, M.T. Mcdowell, Y. Yan, C. Wang, C. Yi, Nano Lett. 12 (2012) 3315–3321.
[83] L. Hu, H. Wu, S.S. Hong, L. Cui, J.R. Mcdonough, S. Bohy, Y. Cui, Chem. Commun. 47 (2011) 367–369.
[84] L.F. Cui, R. Ruffo, C.K. Chan, H. Peng, Y. Cui, Nano Lett. 9 (2009) 491–495.
[85] L.F. Cui, L. Hu, J.W. Choi, Y. Cui, ACS Nano 4 (2010) 3671–3678.
[86] M. Pharr, Z. Suo, J.J. Vlassak, Nano Lett. 13 (2013) 5570–5577.
[87] F. Shi, Z. Song, P.N. Ross, G.A. Somorjai, R.O. Ritchie, K. Komvopoulos, Nat. Commun. 7 (2016) 11886.
[88] N.P. Wagner, K. Asheim, F. Vullum-Bruer, A.M. Svensson, J. Power Sources 437 (2019) 226884.
[89] C. Yu, X. Chen, Z. Xiao, C. Lei, C. Zhang, X. Lin, B. Shen, R. Zhang, F. Wei, Nano Lett. 19 (2019) 5124–5132.
[90] C. Zhao, T. Wada, V. De Andrade, D. Gürsoy, H. Kato, Y.-c.K. Chen-Wiegart, Nano Energy 52 (2018) 381–390.
[91] J. Ryu, T. Chen, T. Bok, G. Song, J. Ma, C. Hwang, L. Luo, H.-K. Song, J. Cho, C. Wang, Nat. Commun. 9 (2018) 2924.
[92] Z. Zheng, B. Chen, N. Fritz, Y. Gurumukhi, J. Cook, M.N. Ates, N. Miljkovic, P.V. Braun, P. Wang, J. Electrochem. Soc. 166 (2019) A2083–A2090.
[93] D. Lyu, B. Ren, S. Li, Acta Mech. 230 (2019) 701–727.
[94] D.E. Galvez-Aranda, J.M. Seminario, J. Electrochem. Soc. 165 (2018) A717–A730.
[95] M.T. McDowell, S.W. Lee, J.T. Harris, B.A. Korgel, C. Wang, W.D. Nix, Y. Cui, Nano Lett. 13 (2013) 758–764.
[96] X.H. Liu, L. Zhong, S. Huang, S.X. Mao, T. Zhu, J.Y. Huang, ACS Nano 6 (2012) 1522–1531.
[97] S.W. Lee, M.T. Mcdowell, L.A. Berla, W.D. Nix, Y. Cui, Proc. Natl. Acad. Sci. 109 (2012) 4080–4085.
[98] Z. Zeng, N. Liu, Q. Zeng, S.W. Lee, W.L. Mao, Y. Cui, Nano Energy 22 (2016) 105–110.
[99] B. Key, R. Bhattacharyya, M. Morcrette, V. Seznec, J.M. Tarascon, C.P. Grey, J. Am. Chem. Soc. 131 (2009) 9239–9249.
[100] J. Duay, K.W. Schroder, S. Murugesan, K.J. Stevenson, ACS Appl. Mater. Interfaces 8 (2016) 17642–17650.
[101] A. Bordes, E. De Vito, C. Haon, A. Boulineau, A. Montani, P. Marcus, Chem. Mater. 28 (2016) 1566–1573.
[102] M.N. Obrovac, V.L. Chevrier, Chem. Rev. 114 (2014) 11444–11502.
[103] T. Kim, S. Park, S.M. Oh, J. Electrochem. Soc. 154 (2007) A1112–A1117.
[104] G. Bieker, M. Winter, P. Bieker, Phys. Chem. Chem. Phys. 17 (2015) 8670–8679.
[105] Q. Pang, A. Shyamsunder, B. Narayanan, C.Y. Kwok, L.A. Curtiss, L.F. Nazar, Nature Energy 3 (2018) 783–791.
[106] P. Zhang, J. Zhu, M. Wang, N. Imanishi, O. Yamamoto, Electrochem. Commun. 87 (2018) 27–30.
[107] F. Wu, Y.-X. Yuan, X.-B. Cheng, Y. Bai, Y. Li, C. Wu, Q. Zhang, Energy Storage Mater. 15 (2018) 148–170.
[108] S.-H. Yu, X. Huang, J.D. Brock, H.D. Abruña, J. Am. Chem. Soc. 141 (2019) 8441–8449.
[109] K. Shen, Z. Wang, X. Bi, Y. Ying, D. Zhang, C. Jin, G. Hou, H. Cao, L. Wu, G. Zheng, Y. Tang, X. Tao, J. Lu, Adv. Energy Mater. 9 (2019) 1900260.

[110] C. Brissot, M. Rosso, J.N. Chazalviel, P. Baudry, S. Lascaud, Electrochim. Acta 43 (1998) 1569–1574.
[111] X.H. Liu, L. Zhong, L.Q. Zhang, A. Kushima, S.X. Mao, J. Li, Z.Z. Ye, J.P. Sullivan, J.Y. Huang, Appl. Phys. Lett. 98 (2011) 183107.
[112] H. Ghassemi, M. Au, N. Chen, P.A. Heiden, R.S. Yassar, Appl. Phys. Lett. 99 (2011) 123113.
[113] Y. Li, Y. Li, A. Pei, K. Yan, Y. Sun, C.L. Wu, L.M. Joubert, R. Chin, A.L. Koh, Y. Yu, J. Perrino, B. Butz, S. Chu, Y. Cui, Science 358 (2017) 506–510.
[114] M.J. Zachman, Z. Tu, S. Choudhury, L.A. Archer, L.F. Kourkoutis, Nature 560 (2018) 345–349.
[115] C. Fang, J. Li, M. Zhang, Y. Zhang, F. Yang, J.Z. Lee, M.-H. Lee, J. Alvarado, M.A. Schroeder, Y. Yang, B. Lu, N. Williams, M. Ceja, L. Yang, M. Cai, J. Gu, K. Xu, X. Wang, Y.S. Meng, Nature 572 (2019) 511–515.
[116] X.R. Liu, X. Deng, R.R. Liu, H.J. Yan, Y.G. Guo, D. Wang, L.J. Wan, ACS Appl. Mater. Interfaces 6 (2014) 20317–20323.
[117] K. Ogata, E. Salager, C.J. Kerr, A.E. Fraser, C. Ducati, A.J. Morris, S. Hofmann, C.P. Grey, Nat. Commun. 5 (2014) 3217.
[118] C. He, S. Wu, N. Zhao, C. Shi, E. Liu, J. Li, ACS Nano 7 (2013) 4459–4469.
[119] B. Wang, X. Li, X. Zhang, B. Luo, M. Jin, M. Liang, S.A. Dayeh, S.T. Picraux, L. Zhi, ACS Nano 7 (2013) 1437–1445.
[120] H. Jia, P. Gao, J. Yang, J. Wang, Y. Nuli, Z. Yang, Adv. Energy Mater. 1 (2011) 1036–1039.
[121] J. Hassoun, B. Scrosati, Angew. Chem. 49 (2010) 2371–2374.
[122] Y.Q. Wang, L. Gu, Y.G. Guo, H. Li, X.Q. He, S. Tsukimoto, Y. Ikuhara, L.J. Wan, J. Am. Chem. Soc. 134 (2012) 7874–7879.
[123] T.H. Hwang, M.L. Yong, B.S. Kong, J.S. Seo, J.W. Choi, Nano Lett. 12 (2011) 802–807.
[124] W. Hui, C. Yi, Nano Today 7 (2012) 414–429.
[125] M. Lebrón-Colón, M.A. Meador, D. Lukco, F. Solá, J. Santos-Pérez, L.S. McCorkle, Nanotechnology 22 (2011) 455707.
[126] S.J. An, J. Li, C. Daniel, D.L. Wood, J. Electrochem. Soc. 166 (2019) A1121–A1126.
[127] S. Dalavi, P. Guduru, B.L. Lucht, J. Electrochem. Soc. 159 (2012) A642–A646.
[128] J. Song, M. Zhou, R. Yi, T. Xu, M.L. Gordin, D. Tang, Z. Yu, M. Regula, D. Wang, Adv. Funct. Mater. 24 (2015) 5904–5910.
[129] A. Magasinski, P. Dixon, B. Hertzberg, A. Kvit, J. Ayala, G. Yushin, Nat. Mater. 9 (2010) 353–358.
[130] N. Liu, Z. Lu, J. Zhao, M.T. McDowell, H.W. Lee, W. Zhao, Y. Cui, Nat. Nanotechnol. 9 (2014) 187–192.
[131] Q. Xu, J.-Y. Li, J.-K. Sun, Y.-X. Yin, L.-J. Wan, Y.-G. Guo, Adv. Energy Mater. 7 (2017) 1601481.
[132] J. Wu, H. Zeng, X. Li, X. Xiang, Y. Liao, Z. Xue, Y. Ye, X. Xie, Adv. Energy Mater. 8 (2018) 1802430.
[133] X. Shen, Y. Li, T. Qian, J. Liu, J. Zhou, C. Yan, J.B. Goodenough, Nat. Commun. 10 (2019) 900.
[134] X. Wang, W. Zeng, L. Hong, W. Xu, H. Yang, F. Wang, H. Duan, M. Tang, H. Jiang, Nature Energy 3 (2018) 227–235.
[135] S. Chu, Y. Cui, N. Liu, Nat. Mater. 16 (2016) 16–22.
[136] W. Liu, Z. Chen, G. Zhou, Y. Sun, H.R. Lee, C. Liu, H. Yao, Z. Bao, Y. Cui, Adv. Mater. 28 (2016) 3578–3583.
[137] G.M. Koenig, I. Belharouak, H. Deng, Y.K. Sun, K. Amine, Chem. Mater. 23 (2016) 2863–2870.
[138] S. Abada, G. Marlair, A. Lecocq, M. Petit, V. Sauvant-Moynot, F. Huet, J. Power Sources 306 (2016) 178–192.
[139] H.J. Kim, S. Choi, S.J. Lee, M.W. Seo, J.G. Lee, E. Deniz, Y.J. Lee, E.K. Kim, J.W. Choi, Nano Lett. 16 (2016) 282–288.
[140] M. Ge, J. Rong, X. Fang, C. Zhou, Nano Lett. 12 (2012) 2318–2323.
[141] H. Wu, G. Zheng, N. Liu, T.J. Carney, Y. Yang, Y. Cui, Nano Lett. 12 (2012) 904–909.
[142] N. Nitta, F. Wu, J.T. Lee, G. Yushin, Mater. Today 18 (2015) 252–264.

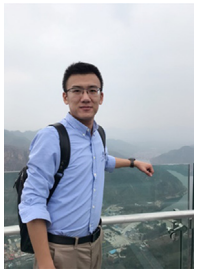

Xiangqi Meng is currently a PhD student at Tianjin University and he is also a joint PhDttars student at Institute of Process Engineering, Chinese Academy of Sciences. His research is supervised by Prof. Hongbin Cao and Prof. Zhi Sun. He received his B.Sc. degree from Tianjin University in 2013. His research interests consist of the failure mechanism and regeneration of electrodes for the lithium-ion batteries.

Hongbin Cao is a professor in Institute of Process Engineering, Chinese Academy of Sciences, deputy director of the National Engineering Laboratory for Hydrometallurgical Cleaner Production Technology and director of Beijing Engineering Research Center of Process Pollution Control. His research interest is the whole process control of industrial pollution: theory, technology and application. Dr. Cao has published over 100 papers, and applied over 60 patents including 5 international patents. He is the holder of the National Science Fund for Distinguished Young Scholars of China (2014).

Yi Zhang is a professor in Institute of Process Engineering, Chinese Academy of Sciences. She is a member of the Chinese Academy of Engineering (since 1999). Her research interest is the green process engineering: theory, technology and application. Professor Zhang has published over 700 papers, and applied over 200 patents.

Zhi Sun is a professor in the Institute of Process Engineering, Chinese Academy of Sciences. His current research focuses on electronic waste treatment, sustainable process design for metal recycling and green design of electronic products. Dr. Sun has coauthored more than 50 publications and 5 patents. He is also editorial board member of two international journals.